Monthly Notices of the ROYAL ASTRONOMICAL SOCIETY
MNRAS **441,** 1934–1942 (2014) doi:10.1093/mnras/stu698

Pre-merger localization of eccentric compact binary coalescences with second-generation gravitational-wave detector networks

Koutarou Kyutoku[1]★ and Naoki Seto[2]

[1]*Department of Physics, University of Wisconsin-Milwaukee, PO Box 413, Milwaukee, WI 53201, USA*
[2]*Department of Physics, Kyoto University, Kyoto 606-8502, Japan*

Accepted 2014 April 7. Received 2014 March 26; in original form 2013 December 10

ABSTRACT

We study the possibility of pre-merger localization of eccentric compact binary coalescences by second-generation gravitational-wave detector networks. Gravitational waves from eccentric binaries can be regarded as a sequence of pulses, which are composed of various higher harmonic modes than ones with twice the orbital frequency. The higher harmonic modes from a very early inspiral phase will not only contribute to the signal-to-noise ratio, but also allow us to localize the gravitational-wave source before the merger sets in. This is due to the fact that high-frequency gravitational waves are essential for the source localization via triangulation by ground-based detector networks. We found that the single-detector signal-to-noise ratio exceeds 5 at 10 min before the merger for a 1.4–1.4 $M_\odot$ eccentric binary neutron stars at 100 Mpc in optimal cases, and it can be localized up to 10 deg^2 at half a minute before the merger by a four-detector network. We will even be able to achieve $\sim$10 deg^2 at 10 min before the merger for a face-on eccentric compact binary by a five-detector network.

Key words: gravitational waves – methods: data analysis – binaries: close – stars: neutron.

1 INTRODUCTION

Gravitational waves from compact binary coalescences are expected to be detected in the coming decade by second-generation gravitational-wave detectors like Advanced LIGO, Advanced Virgo, and KAGRA (Harry & LIGO Scientific Collaboration 2010; Accadia et al. 2011; Somiya 2012). Gravitational waves will give us a way to infer masses and spins of binary components, and also equations of state for supranuclear-density matter if the binary involves a neutron star. In addition to these intrinsic parameters, extrinsic parameters such as the luminosity distance and sky position of the binary can also be studied by gravitational-wave observation. Once we localize a compact binary coalescence in the sky to the extent that the host galaxy is determined, the luminosity distance will be known as a function of the cosmological redshift so that a new distance ladder may be constructed (Schutz 1986). Electromagnetic counterparts of compact binary coalescences are also important at this stage (Metzger & Berger 2012; Piran, Nakar & Rosswog 2013), because seeing them is more advantageous for accurate localization than hearing gravitational waves.

One ambitious goal of gravitational-wave astronomy is to sound a merger alert before the merger sets in. The benefit of realtime electromagnetic observation of the compact binary merger will be immeasurable. Nearly simultaneous detection of gravitational and electromagnetic waves will give us an opportunity to investigate the propagation speed of gravitational waves as SN 1987A did for neutrinos (Bionta et al. 1987; Hirata et al. 1987). Realtime observation of the merger is also useful to understand electromagnetic radiation mechanisms. If short-hard gamma-ray bursts are driven by compact binary coalescences (see Nakar 2007; Berger 2013 and references therein for reviews), we will be able to detect prompt emission from the beginning in various wavelengths for face-on compact binaries. Recent possible 'kilonova' detection supports this binary merger scenario of the short-hard gamma-ray burst (Berger, Fong & Chornock 2013; Hotokezaka et al. 2013; Tanvir et al. 2013), and we can reasonably expect simultaneous detection with gravitational waves. Still, direct connection between the short-hard gamma-ray bursts and gravitational waves is essential for the robust confirmation of the scenario. The onset of afterglow will be observed following the prompt emission. Extended emission observed in the afterglow is one of the most mysterious feature of the short-hard gamma-ray bursts (e.g. Nakamura et al. 2013; Veres & Mészáros 2013), and detailed characteristics including its opening angle will be investigated if a merger alert could be sounded. Other electromagnetic events involving ultrarelativistic outflows, such as a proposed shock breakout emission from binary neutron star mergers (Kyutoku, Ioka & Shibata 2014), are also easier to detect with realtime observation.

Besides the signal-to-noise ratio (SNR), localization of the gravitational-wave source up to moderate accuracy is necessary for successful follow-up detection of electromagnetic counterparts

★E-mail: kyutoku@uwm.edu

(Nissanke, Kasliwal & Georgieva 2013; LIGO Scientific Collaboration and Virgo Collaboration 2013), and thus pre-merger localization should be regarded as a prerequisite for generating merger alerts. Pointing only known galaxies using available catalogues will help to detect electromagnetic counterparts particularly in the early era of gravitational-wave astronomy (Nuttall & Sutton 2010). Still, assuming the number density of galaxies to be 0.01 Mpc^{-3}, $\sim$8 galaxies per deg^2 will be found if we are going to observe out to $\sim$200 Mpc. Thus, accurate localization is eagerly desired irrespective of our follow-up strategy.

Detection and localization of circular binaries on the celestial sphere prior to the merger are challenging tasks (Abadie et al. 2012; Cannon et al. 2012; Evans et al. 2012), whereas such binaries will be the most frequent sources and are extensively studied. The reason for this is that a circular binary has the largest periapsis distance for a fixed value of the semimajor axis, and the luminosity averaged over an orbit is the lowest among possible configurations. Furthermore, gravitational-wave frequency is only twice the orbital frequency within the quadrupole approximation. The localization of gravitational-wave sources is primarily based on triangulation via the timing difference between detectors (Fairhurst 2011). Typical separations of ground-based detectors determine typical timing differences $O(10)$ ms, and thus accurate localization requires gravitational waves with frequency higher than $\sim$100 Hz. But, the gravitational-wave frequency from 1.4–1.4 $\mathrm{M}_\odot$ binary neutron stars in a circular orbit does not reach 10 Hz until $\sim$1000 s before the merger, and reaches 100 Hz only at $\sim$2 s before the merger. As a result, the area of the 90 per cent localization confidence will be larger than 100 deg^2 even 1 s before the merger for typical events (Cannon et al. 2012). Moreover, the SNR does not substantially accumulate until gravitational-wave frequency reaches $\sim$100 Hz, because each detector is sensitive around 100 Hz. Taking a few to 10 min of latency associated with trigger and alert generation into account (Cannon et al. 2012), it would be challenging to sound merger alerts with second-generation detector networks even if we could omit human validation processes. Furthermore, practical target-of-opportunity observation will involve overheads of telescopes and satellites as additional latency sources.

The situation could be changed for eccentric compact binary coalescences (e.g. O'Leary, Kocsis & Loeb 2009), which emit higher mode gravitational waves even within the quadrupole approximation (Peters & Mathews 1963). Event rates of eccentric compact binary coalescences are conceivably low, and several authors investigated this possibility. Note that the horizon distance $\sim$200 Mpc of a single detector is not changed drastically by the presence of a finite eccentricity unless the binary is formed with an extremely short periapsis distance as we discuss later. Lee, Ramirez-Ruiz & van de Ven (2010) studied the formation of very hard eccentric binaries via tidal-interaction induced captures in globular clusters focusing on nearly direct collisions. They found that the local formation rate of binary neutron stars may be a few tens Gpc^{-3} yr^{-1} depending on globular cluster models. Although this rate is motivating for ground-based detectors, East et al. (2013) pointed out that this might be an order-of-magnitude overestimation caused by assuming extremely high retention fraction of neutron stars (see also Tsang 2013). At the same time, East et al. (2013) also pointed out that the cross-section of gravitational-wave induced captures is larger than that of the tidal-interaction ones by an order of magnitude. Indeed, whereas the tidal capture requires the initial periapsis distance to be smaller than $r_{\mathrm{p,\,max}} \approx 30$–$40GM/c^2$ for binary neutron stars with the total mass M, where G and c are the gravitational constant and speed of light, respectively (Lee et al. 2010), the gravitational-wave capture can work up to $r_{\mathrm{p,\,max}} \approx 600$–$700GM/c^2$ irrespective of the binary components (O'Leary et al. 2009). Thus, the merger rate of eccentric binary neutron stars could be $\sim$1 yr^{-1} within the sensitive volume of second-generation gravitational-wave detectors. Here, we would not say that such eccentric compact binary coalescences are frequent enough, because the rate estimation is not settled.[1] Instead, we consider that they can be possible events and should not be completely neglected in the gravitational-wave data analysis. Note that an eccentric binary formed with a very large periapsis distance r_{p} essentially circularizes before gravitational waves are detected, where the distribution of r_{p} is expected to be flat below $r_{\mathrm{p,\,max}}$ from the fact that the capture cross-section is proportional to r_{p}.

In this paper, we explore a possibility of realtime detection and localization of moderately eccentric compact binary coalescences. Here, we use the word 'moderately eccentric' to state that the binary is eccentric during a detectable inspiral phase, and circularized to a low value of eccentricity, say $e \lesssim 0.1$, when it reaches the last stable orbit. In such cases, the remnant of the merger and associated electromagnetic counterparts are expected to be more similar to those of circular compact binary coalescences than those of direct collisions. We only focus on equal-mass, 1.4–1.4 $\mathrm{M}_\odot$ binary neutron stars in this study, and our result depends only weakly on the total mass and mass ratio once effects of the eccentricity are properly normalized with respect to the chirp mass. We always assume that binary components are treated as non-spinning point particles up to the last stable orbit, while the exact merger is determined by the radius of neutron stars.

The paper is organized as follows. In Section 2, we briefly summarize the orbital evolution of eccentric binaries. Next, in Section 3, our formalism to evaluate the SNR, timing accuracy, and localization accuracy is described. Results are shown in Section 4, and Section 5 is devoted to the summary and discussion. We denote masses of each component by m_1 and m_2. The total mass and reduced mass are written by $M = m_1 + m_2$ and $\mu = m_1 m_2/M$, respectively. The distance to the binary from the earth (or Solar system barycentre) is written by D. The semimajor axis and eccentricity of the binary are denoted by a and e, respectively.

2 BINARY EVOLUTION

We describe the motion of an eccentric binary with a and e in Newtonian gravity, and consider gravitational radiation in terms of quadrupole formula. The orbital frequency as the inverse of the period is given by

$$f_{\mathrm{orb}}(a) = \frac{1}{2\pi}\sqrt{\frac{GM}{a^3}}, \tag{1}$$

and gravitational waves are decomposed into harmonic modes with frequency

$$f_n = n f_{\mathrm{orb}}, \tag{2}$$

[1] It is suggested that dynamical binary-stellar encounters could be another efficient channel of eccentric compact binary formation (Samsing, Macleod & Ramirez-Ruiz 2014). It is also suggested that the Kozai mechanism in hierarchical triples could reduce the time to the merger of inner compact binaries by several orders of magnitude, and enhance the merger rate (Antonini & Perets 2012; Seto 2013; Antognini et al. 2014).

where $n \geq 1$ (Peters & Mathews 1963). The luminosity of each harmonic mode averaged over an orbit is given by

$$\frac{\mathrm{d}E_n}{\mathrm{d}t} = -\frac{32}{5}\frac{G^4M^3\mu^2}{c^5a^5}g(n,e), \tag{3}$$

where $g(n, e)$ is given by equation 20 of Peters & Mathews (1963). We have

$$\sum_{n=1}^{\infty} g(n,e) = \frac{1+(73/24)e^2+(37/96)e^4}{(1-e^2)^{7/2}} = g(e), \tag{4}$$

and the total luminosity averaged over an orbit $\mathrm{d}E/\mathrm{d}t$, which governs the orbital evolution, is given in terms of $g(e)$.

Time evolution of an eccentric binary due to radiation reaction is handled following O'Leary et al. (2009) in this study. Specifically, we use the eccentricity, e, as the independent variable, and describe all quantities including the time to the merger as functions of e. The time evolution of a and e are derived under the assumption of adiabatic evolution according to Peters (1964), whereas the actual evolution may be more discontinuous due to the pulse-like nature of gravitational waves from a highly eccentric binary. This approximation may require sophistication once we are going to prepare waveform templates, and we do not expect that it changes the story as far as pulse-like gravitational-wave trains are emitted.

The periapsis distance is given by $r_\mathrm{p} = a(1-e)$, and we introduce a normalized periapsis distance

$$\hat{r}_\mathrm{p} \equiv \frac{a(1-e)}{GM/c^2}, \tag{5}$$

for convenience. We further introduce an initial normalized periapsis distance at $e = 1$ as $\hat{r}_{\mathrm{p}0}$. Although realistic binaries should be formed with an eccentricity smaller than unity, we consider the evolution of a binary from $e = 1$ as an approximation. This approximation can be relaxed by evolving a binary from a realistic initial value at $e_\mathrm{i} < 1$, but we do not take this step so that the formation process is kept unspecified. The change of quantities such as SNRs associated with setting $e_\mathrm{i} = 1$ is negligible due to its proximity to unity if we assume gravitational-wave induced captures (see Fig. 1).

The periapsis distance evolves in time according to (O'Leary et al. 2009)

$$\hat{r}_\mathrm{p}(e) = \hat{r}_{\mathrm{p}0}\kappa(e), \tag{6}$$

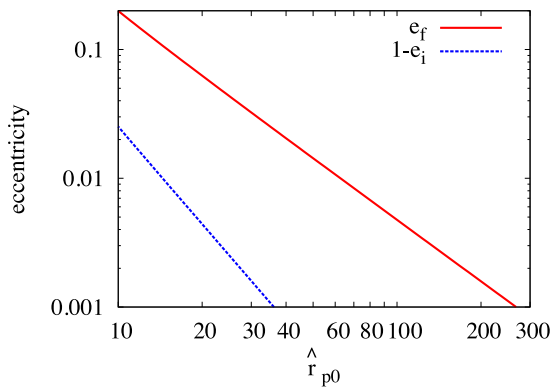

Figure 1. The eccentricity at the last stable orbit e_f (Cutler, Kennefick & Poisson 1994) and deviation of initial eccentricity from the unity $1 - e_\mathrm{i}$ for a gravitational-wave induced capture as functions of the initial periapsis distance, $\hat{r}_{\mathrm{p}0}$ (O'Leary et al. 2009).

where

$$\kappa(e) = 2\left(\frac{304}{425}\right)^{870/2299}\frac{e^{12/19}}{1+e}\left(1+\frac{121}{304}e^2\right)^{870/2299}. \tag{7}$$

This implies that

$$a(e) = \frac{\hat{r}_{\mathrm{p}0}GM}{c^2}\frac{\kappa(e)}{1-e}, \tag{8}$$

$$f_\mathrm{orb}(e) = \frac{c^3}{2\pi GM}\left(\frac{1-e}{\hat{r}_{\mathrm{p}0}\kappa(e)}\right)^{3/2}. \tag{9}$$

The formal time to the merger, at which $e = 0$ is achieved, is given by

$$t_\mathrm{m}(e) = \frac{15}{19}\left(\frac{304}{425}\right)^{3480/2299}\frac{\hat{r}_{\mathrm{p}0}^4GM^2}{c^3\mu} \times \int_0^e \frac{e'^{48/19}}{(1-e'^2)^{3/2}}\left(1+\frac{121}{304}e'^2\right)^{1181/2299}\frac{\mathrm{d}e'}{e'}. \tag{10}$$

We use this to denote the time to the merger, whereas we truncate gravitational radiation at a finite eccentricity e_f of the last stable orbit, at which

$$\hat{r}_\mathrm{p}(e_\mathrm{f}) = \frac{6+2e_\mathrm{f}}{1+e_\mathrm{f}} \tag{11}$$

is achieved (Cutler et al. 1994; Barack & Cutler 2004).

Fig. 1 shows the value of e_f as a function of $\hat{r}_{\mathrm{p}0}$ as well as (deviation from the unity of) the initial eccentricity

$$e_\mathrm{i} \approx \left(1-\frac{85\pi\mu}{3\sqrt{2}\hat{r}_{\mathrm{p}0}^{5/2}M}\right)^{1/2} \tag{12}$$

for a gravitational-wave induced capture as an example formation process (O'Leary et al. 2009). The eccentricity at the merger, which may correspond roughly to that at the last stable orbit, is less than 0.1 for $\hat{r}_{\mathrm{p}0} \gtrsim 15$, and thus we expect that the merger outcome and electromagnetic counterparts are closer to those for circular cases than those for direct collisions. The time to the merger from the initial eccentricity $e_\mathrm{i} \approx 1$ is

$$t_\mathrm{m}(e_\mathrm{i}) \approx \frac{3c^5}{85G^3M^2\mu}a(e_\mathrm{i})^4\left(1-e_\mathrm{i}^2\right)^{7/2} \tag{13}$$

$$\propto \hat{r}_{\mathrm{p}0}^{21/4}, \tag{14}$$

and this is approximately twice the orbital period at the formation, which is also proportional to $\hat{r}_{\mathrm{p}0}^{21/4}$. Here, formation via the gravitational-wave induced capture is assumed and equation (12) is used. The specific values of $t_\mathrm{m}(e_\mathrm{i})$ are half an hour, ∼3 d, and ∼3 yr for $\hat{r}_{\mathrm{p}0} = 40$, 100, and 300, respectively. Since the orbital period, which is proportional to $a^{3/2}$, after N periastron passages decreases as $1/N^{3/2}$ in a high-eccentricity regime, more than 10 orbits are always expected as far as the binary is formed with $e_\mathrm{i} \approx 1$. This may validate the use of the adiabatic approximation, whereas the discontinuous nature of eccentric binary evolution should be considered seriously in practice, especially for binaries formed with small values of $r_{\mathrm{p}0}$.

3 DATA ANALYSIS

We estimate the localization accuracy of a gravitational-wave source adopting the timing triangulation approximation (Fairhurst 2009; Grover et al. 2014). In this approximation, the source position is

reconstructed geometrically using the difference of gravitational-wave arrival times among detectors in a network. The localization accuracy is primarily determined by the timing accuracy in each detector. In this section, we describe computations of 'realtime' SNRs, timing accuracy, and localization accuracy, aiming at pre-merger localization.

3.1 Signal-to-noise ratio

One of the most important statistics in gravitational-wave data analysis is the SNR at a single detector. We always assume that the matched-filtering analysis is conducted. To circumvent complexities associated with the sky position and orientation of a binary with respect to the detector, we express relevant integrals in terms of the luminosity as an averaged quantity following Flanagan & Hughes (1998), O'Leary et al. (2009) and Kocsis & Levin (2012). For gravitational waves composed of various harmonic modes, the averaged (and optimal) SNR is given by

$$\rho^2 = \sum_{n=1}^{\infty} \rho_n^2 \ , \ \rho_n^2 = \frac{2G}{5\pi^2 c^3 D^2} \int_0^{\infty} \frac{|\mathrm{d}E_n/\mathrm{d}f_n|}{f_n^2 S(f_n)} \mathrm{d}f_n, \tag{15}$$

using the fact that overlaps between different harmonic modes vanish (Barack & Cutler 2004). Here, $S(f)$ is one-sided noise power spectral density of the detector. In this study, we always use the anticipated noise curve of the zero-detuning, high laser power Advanced LIGO configuration (https://dcc.ligo.org/cgi-bin/DocDB/ShowDocument?docid=2974).

To explore the possibility of a realtime merger alert, we extend the SNR to a function of our time variable, i.e. eccentricity.[2] Using a relation $(\mathrm{d}E_n/\mathrm{d}f_n)\mathrm{d}f_n = (\mathrm{d}E_n/\mathrm{d}t)(\mathrm{d}e/\mathrm{d}t)^{-1}\mathrm{d}e$, the realtime SNR for the nth harmonic mode is given by

$$\rho_n^2(e) = \frac{G^3 M^2 \mu \hat{r}_{\mathrm{p0}}^2}{c^7 D^2} \int_e^1 \frac{g(n,e)u(e)}{n^2 S(f_n(e))} \frac{\mathrm{d}e}{e}, \tag{16}$$

where

$$u(e) = \frac{192}{95}\left(\frac{304}{425}\right)^{1740/2299} \times (1-e^2)^{1/2} e^{24/19} \left(1+\frac{121}{304}e^2\right)^{-559/2299}. \tag{17}$$

and $f_n(e) = n f_{\mathrm{orb}}(e)$. The realtime total SNR is given by

$$\rho^2(e) = \sum_{n=1}^{\infty} \rho_n^2(e), \tag{18}$$

and thus, the relation between the SNR $\rho(e)$ and time to the merger $t_{\mathrm{m}}(e)$ is given in a parametrized form. In a practical numerical computation, we truncate the summation at

$$n_{\max}(e) = 5\frac{(1+e)^{1/2}}{(1-e)^{3/2}}, \tag{19}$$

with which 0.1 per cent accuracy is expected to be achieved (O'Leary et al. 2009). The realtime SNR obtains its full value at the last stable orbit as $\rho(e_{\mathrm{f}}) = \rho$.

Because $n_{\max}(e)$ diverges at $e = 1$, we have to approximate the integral at $e \approx 1$. Using the fact that gravitational-wave pulses emitted at $e \approx 1$ are approximately identical, we replace the gravitational-wave luminosity distribution over harmonic modes at any value of e larger than a prescribed value e_{cut} by that at $e = e_{\mathrm{cut}}$, as well as the representative frequency for each harmonic mode. This gives

$$\rho^2(e > e_{\mathrm{cut}}) \approx \frac{2G}{5\pi^2 c^3 D^2} \frac{|\Delta E|}{g(e_{\mathrm{cut}})} \sum_{n=1}^{n_{\max}(e_{\mathrm{cut}})} \frac{g(n, e_{\mathrm{cut}})}{f_n^2(e_{\mathrm{cut}}) S(f_n(e_{\mathrm{cut}}))}, \tag{20}$$

where

$$\Delta E = -\frac{GM\mu}{2a(e_{\mathrm{cut}})} \tag{21}$$

is the energy radiated between $e = 1$ and $e = e_{\mathrm{cut}}$. We typically set $e_{\mathrm{cut}} = 0.995$, and the error associated with this approximation is at most 0.1 per cent, thus negligible. This is because the radiated energy is very small in the relevant regime. Another way to avoid this divergence is to introduce realistic initial values, $e_{\mathrm{i}} < 1$.

3.2 Timing accuracy

For a circular binary, the timing accuracy is often approximated by inverting a two-dimensional Fisher information matrix for the reference time t_0 and phase Φ_0 (e.g. the coalescence time and phase) neglecting the correlation with other parameters (Fairhurst 2009). On one hand, it is known that the amplitude and polarization information of gravitational waves in each detector improve the localization accuracy (Kasliwal & Nissanke 2013). On the other hand, the timing triangulation approximation depends on the Fisher analysis, which is only accurate at large SNRs. In total, the timing triangulation approximation with timing accuracy obtained by the two-dimensional model is found to underestimate the localization accuracy by a factor of $\sim$4 compared to that obtained by fully Bayesian analysis for all the parameters including the sky position at realistic SNRs (Grover et al. 2014).

In this study, we evaluate the timing accuracy simply by a one-dimensional model in which the correlation between the time and all the other parameters are neglected for both circular and eccentric binaries. In the terminology of the Fisher matrix, the timing accuracy is estimated as $\sigma_{\mathrm{t}} = (\Gamma_{tt})^{-1/2}$ using the Fisher matrix component with respect to the reference time. We find that the timing accuracy estimated in this one-dimensional model is exactly the same as the result of a two-dimensional, time-and-phase model for an eccentric binary formed with $e = 1$. This owes to the divergence of the Fisher matrix component $\Gamma_{\Phi\Phi}$ with respect to the reference phase in the limit of $e \to 1$. The correlation term $\Gamma_{t\Phi}(\Gamma_{tt}\Gamma_{\Phi\Phi})^{-1/2}$ vanishes in this limit. Even if the realistic initial eccentricity e_{i} is slightly less than unity, our results are essentially unchanged as the divergence $\Gamma_{\Phi\Phi} \propto (1-e_{\mathrm{i}})^{-2}$ is rapid (see Appendix A). On another front, Grover et al. (2014) show for a circular binary that this approximation gives overestimated accuracy by a factor of $\sim$2 than fully Bayesian analysis, and thus, we assume this as an approximate upper limit. These facts imply that the contrast between localization properties of eccentric and circular binaries elucidated by our one-dimensional model is expected to be a conservative estimation.

The reason of the exquisite accuracy for the reference phase of eccentric binaries is the different morphology of gravitational waves. The gravitational waveform of circular binaries is usually called as a chirp signal, in which only a nearly sinusoidal $n = 2$ mode is emitted with increasing amplitude and frequency throughout their lifetimes within the quadrupole approximation. The matched filtering for this case is essentially a problem of matching the phase evolution. By contrast, gravitational waves from eccentric binaries with $e \approx 1$ are considered as a sequence of nearly identical pulses emitted around

[2] We used Parseval's theorem to derive the expression in terms of the luminosity. Although it may seem inappropriate to truncate the integration with the finite time duration, problems do not occur as long as the adiabatic approximation is valid.

the periapsis, or repeated bursts (Kocsis & Levin 2012). In this case, the matched filtering may be considered as a problem of finding the arrival time of pulse peaks displaced by decreasing orbital periods. The pulse width is approximately constant at $e \approx 1$, whereas the orbital period diverges at $e \to 1$. Thus, the orbital phase is determined accurately to be the periapsis when the pulses are observed.

The Fisher matrix component for the reference time is obtained using the fact that the nth harmonic mode gravitational waves are proportional to $\exp[\mathrm{i}n(2\pi f_{\rm orb}t_0 - \Phi_0)]$ in the frequency domain. It is given by

$$\Gamma_{tt} = (2\pi)^2 \sum_{n=1}^{\infty} \rho_n^2 \overline{f_n^2}, \tag{22}$$

where the mth moment of the frequency for nth harmonic, $\overline{f_n^m}$, is defined by[3] (Fairhurst 2009, 2011)

$$\overline{f_n^m} \equiv \frac{1}{\rho_n^2} \frac{2G}{5\pi^2 c^3 D^2} \int_0^{\infty} \frac{f_n^m |\mathrm{d}E_n/\mathrm{d}f_n|}{f_n^2 S(f_n)} \mathrm{d}f_n. \tag{23}$$

Similarly to the SNR, the realtime mth moment of the frequency for nth harmonic is defined by

$$\overline{f_n^m}(e) = \frac{1}{\rho_n^2(e)} \frac{G^3 M^2 \mu \hat{r}_{\rm p0}^2}{c^7 D^2} \int_e^1 \frac{f_n^m(e) g(n,e) u(e)}{n^2 S(f_n(e))} \frac{\mathrm{d}e}{e}, \tag{24}$$

and the realtime timing accuracy is expressed as

$$\sigma_{\rm t}(e) = \frac{1}{2\pi} \sqrt{\frac{1}{\sum_n \rho_n^2(e) \overline{f_n^2}(e)}}. \tag{25}$$

We again truncate the summation at $n_{\rm max}(e)$. The relation between the timing accuracy $\sigma_{\rm t}(e)$ and time to the merger $t_{\rm m}(e)$ is given in a parametrized form in a similar manner to that between the SNR and timing accuracy.

As already noted, the caveat of this model is that it relies on the Fisher analysis, which breaks down at the low SNR regime. Unfortunately, we are always interested in the low SNR regime as far as our aim is to sound a merger alert as early as possible. Comparisons with the fully Bayesian analysis are conducted in Grover et al. (2014) for a circular binary, but they have never been done for an eccentric binary. Furthermore, the validity in the very low SNR regime required for pre-merger localization is not checked even for circular binaries. Thus, the Fisher analysis could be a poorer approximation in realistic data analysis for pre-merger localization of eccentric binaries than expected from the previous study of a circular binary. We left more quantitative analysis such as the fully Bayesian one for the future study.

3.3 Localization

We follow Fairhurst (2011) to estimate localization ability of a detector network. Localization accuracy depends on a particular configuration of the detector network. In this study, we focus on a four-detector network composed of Advanced LIGO Hanford, Advanced LIGO Livingston, Advanced Virgo, and KAGRA, whereas the expression below is not limited to this particular network. We also consider a five-detector network composed of the mentioned four detectors and LIGO India. Their locations are taken from Schutz (2011). The antenna pattern functions and noise curves will be different among the detectors, but we adopt the same value of $\sigma_{\rm t}(e)$ at all the detectors for simplicity. While we have not critically assessed the deviation from realistic values due to this approximation, we believe that our result is sufficient to elucidate the effect of eccentricity semiquantitatively, partly because $\sigma_{\rm t}(e)$ is derived by averaging over the sky position and orientation of the binary.

Once locations of detectors and timing accuracy at them are determined, the inverse covariance matrix associated with the probability distribution of the sky position is given by (Fairhurst 2011)

$$M_{ij} = \frac{1}{\sum_I \left(1/\sigma_I^2\right)} \sum_{I,J} \frac{D_{i,IJ} D_{j,IJ}}{2c^2 \sigma_I^2 \sigma_J^2}. \tag{26}$$

Here, lowercase Latin indices denote three-dimensional coordinates, and we do not restrict the estimated source position to be on the celestial sphere at this stage. Uppercase Latin indices refer to the detectors in a network. The timing accuracy at the detector I is written by σ_I, and $D_{i,IJ} \equiv d_{i,I} - d_{i,J}$ where $d_{i,I}$ is the location of the detector I. This expression is valid for the case in which the timing accuracy depends on the detector, whereas we adopt common values in this study as stated above. This matrix M_{ij} has three eigenvalues, and they define the inverse squared localization error of the sky position in the three-dimensional space.

We would like to restrict the sky position of the source to the celestial sphere (Fairhurst 2011). The localization error at the sky position (θ, ϕ) is given using the projection matrix

$$P_i{}^j(\theta,\phi) = \delta_i{}^j - n_i(\theta,\phi) n^j(\theta,\phi), \tag{27}$$

where $n_i(\theta, \phi)$ is the unit vector pointing (θ, ϕ) from the centre of the earth. The projected inverse covariance matrix is given by

$$\hat{M}_{ij}(\theta,\phi) = P_i{}^k(\theta,\phi) P_j{}^l(\theta,\phi) M_{kl}, \tag{28}$$

and the two non-zero eigenvalues of this matrix, $\sigma_1(\theta, \phi)$ and $\sigma_2(\theta, \phi)$, determine the localization accuracy around (θ, ϕ). Finally, the localization error $\Delta\Omega$ with a probability p is approximately given by

$$\Delta\Omega(\theta,\phi;p) \approx 2\pi\sigma_1(\theta,\phi)\sigma_2(\theta,\phi)[-\ln(1-p)]. \tag{29}$$

In this study, we search the best and worst localization errors over the sky position (θ, ϕ) for a given detector network, and also take the average.

4 RESULT

First, we demonstrate the dependence of ρ and $\sigma_{\rm t}$ as full values, i.e. those obtained after all the radiation are detected, on the initial periapsis distance $\hat{r}_{\rm p0}$ in Fig. 2. For comparison, all the values are normalized with respect to those of a circular binary, which take $\rho = 14.2$ and $\sigma_{\rm t} = 0.072$ ms for a binary at $D = 100$ Mpc. Fig. 3 shows the relative difference in the logarithmic scale, and representative values for selected eccentric binaries as well as those for circular binaries are shown in Table 1.

The SNR, ρ, takes the largest value at $\hat{r}_{\rm p0} \approx 88$. This increase of the SNR at moderately large $\hat{r}_{\rm p0}$ is primarily ascribed to the fact that the radiated energy tends to concentrate around sensitive frequency of a particular detector configuration. In contrast, the SNR decreases at smaller values of $\hat{r}_{\rm p0}$, because the initial orbit is too close to the last stable orbit and contribution from the inspiral phase at a large separation is lost. For a large value of $\hat{r}_{\rm p0} \gtrsim 300$, the SNR is essentially the same as that of a circular binary. This figure implies that the horizon distance is changed only up to a few tens per cent for eccentric binaries except for those born with very small $\hat{r}_{\rm p0}$. We do not pay particular attention to such a weak signal regime in this study.

[3] We separate $1/\rho_n^2$ in $\overline{f_n^m}$ and ρ_n^2 to match the existing study for a circular binary.

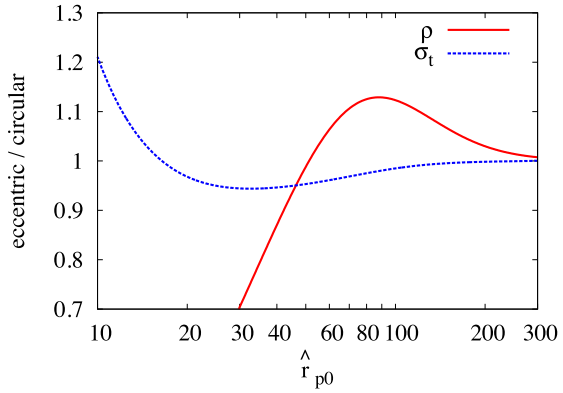

Figure 2. The dependence of ρ and σ_t for a single detector on $\hat{r}_{p0}$. A 1.4–1.4 $M_\odot$ binary is assumed. The values are normalized with respect to those of circular binaries, where σ_t is defined by $(\Gamma_{tt})^{-1/2}$.

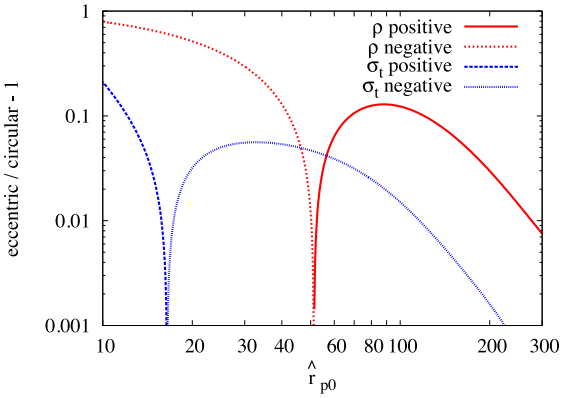

Figure 3. The relative difference of ρ and σ_t for a single detector compared to the values of circular binaries. A 1.4–1.4 $M_\odot$ binary is assumed. The values larger and smaller than those of a circular binary are denoted by positive and negative, respectively. For better localization, ρ and σ_t should be larger (ρ positive) and smaller (σ_t negative), respectively.

Table 1. The SNR ρ and timing accuracy σ_t for a single detector of a 1.4 $M_\odot$–1.4 $M_\odot$ binary at $D = 100$ Mpc with various values of $\hat{r}_{p0}$. These for a circular binary are also presented as $\hat{r}_{p0} = \infty$. The timing accuracy of a circular binary in the one-dimensional model shown in this table is better by 23 per cent than 93.2 μs obtained in the two-dimensional model including the phase.

$\hat{r}_{p0}$	ρ	σ_t (μs)
40	12.4	67.7
100	16.0	70.7
300	14.3	71.7
∞	14.2	71.8

The timing accuracy for an eccentric binary with $\hat{r}_{p0} \gtrsim 15$ is better than that for a circular binary, and it approaches the value for a circular binary at large $\hat{r}_{p0}$. We stress that the values for eccentric and circular binaries agree when we focus only on the reference time, and the results deviate even in the limit of $\hat{r}_{p0} \to \infty$ when we also consider the reference phase. The timing accuracy becomes worse than that of the circular binary at $\hat{r}_{p0} \lesssim 15$ due to the lack of the SNR, and we do not pay attention to that regime. The best timing accuracy is achieved at $\hat{r}_{p0} \approx 32$, whereas the SNR is smaller by ∼30 per cent than the circular value.

Next, we compare time evolution of ρ and σ_t between eccentric and circular binaries. Fig. 4 shows the time evolution of ρ and σ_t for various values of $\hat{r}_{p0}$ as well as those for a circular binary at $D = 100$ Mpc. As an eyeguide, we include horizontal lines which denote $\rho = 8$ both for the orientation-averaged and face-on binaries. Here, we also show the scale for face-on binaries, because the short-hard gamma-ray burst should be more relevant for such cases.

The comparison of the SNR evolution shows that eccentric binary coalescences accumulate SNRs from earlier stages of their lifetimes. A circular binary at $D = 100$ Mpc achieves $\rho = 8$ only at ∼20 s before the merger. By contrast, an eccentric binary with $\hat{r}_{p0} = 100$ does at ∼100 s before the merger, partly due to the large full SNR but mainly due to strong emission at an early stage of its evolution. If we consider $\rho = 5$ or $\rho = 8$ of a face-on binary as a triggering criterion of the merger alert, it is achieved at ∼10 min before the merger for $\hat{r}_{p0} = 100$, whereas it is ∼1 min for a circular binary. The rapid SNR accumulation at a few minutes before the merger occurs approximately for $50 \lesssim \hat{r}_{p0} \lesssim 200$. For a large value of $\hat{r}_{p0} \gtrsim 300$, the accumulation behaviour of the SNR approach asymptotically to that of the circular case, because the dominant emission channel becomes the $n = 2$ mode from a close orbit. For a small value of $\hat{r}_{p0} \lesssim 30$, the SNR is not substantial.

The time evolution of timing accuracy also depends on the value of $\hat{r}_{p0}$. For a circular binary, $\sigma_t = 1$ ms is achieved at only ∼40 s before the merger with $\rho = 6$. By contrast, an eccentric binary with $\hat{r}_{p0} = 100$ can achieve the same accuracy at ∼12 min before the merger. Roughly speaking, $\sigma_t = 1$ ms is achieved at a few minutes before the merger for $50 \lesssim \hat{r}_{p0} \lesssim 150$. For virtually all the cases, the timing accuracy as a function of the time to the merger is always better for an eccentric binary than for a circular binary, while the SNR can be smaller for a small value of $\hat{r}_{p0}$. This reflects the fact that the localization depends crucially on high-frequency gravitational waves, which a circular binary does not emit until right before the merger.

Finally, we compare time evolution of the localization accuracy between eccentric and circular binaries. Fig. 5 shows the evolution of localization accuracy for various values of $\hat{r}_{p0}$ as well as that for a circular binary. The localization area is shown as a sky position averaged value, and the best (worst) case values are obtained by multiplying 0.4 (3) and 0.5 (2.5) for four- and five-detector networks considered here, respectively (see Table 2). Although we specify a detector network, we do not take directional dependence of the antenna pattern function of each detector into account, and we take the same values of σ_t at all the detectors for simplicity. These values depend on the orientation and sky position of the binary and also orientation of the detector in reality. Especially, adopting the same values in all the detectors does not give realistic results for cases in which a binary is located on blind spots of detectors. Thus, this figure should not be taken too quantitatively, while we believe that this approximation is sufficient to demonstrate the localization efficiency.

This figure suggests that eccentric binaries could be localized with 68 per cent confidence up to ∼10 deg^2, typical field of view of large-area optical telescopes (Nissanke et al. 2013), at half a minute before the merger by a four-detector network. On the other hand, a circular binary can be localized up to this accuracy only at a few seconds before the merger. If lower confidence and/or larger localization error are allowed for the purpose of sounding merger alerts, more rapid localization is possible.

Taking the expected latency for a gravitational-wave data analysis pipeline, one interesting value may be those at 10 min before the merger, at which $\rho = 5$, $\sigma_t = 1$ ms and $\Delta\Omega \sim 100\,\mathrm{deg}^2$ at 68 per cent

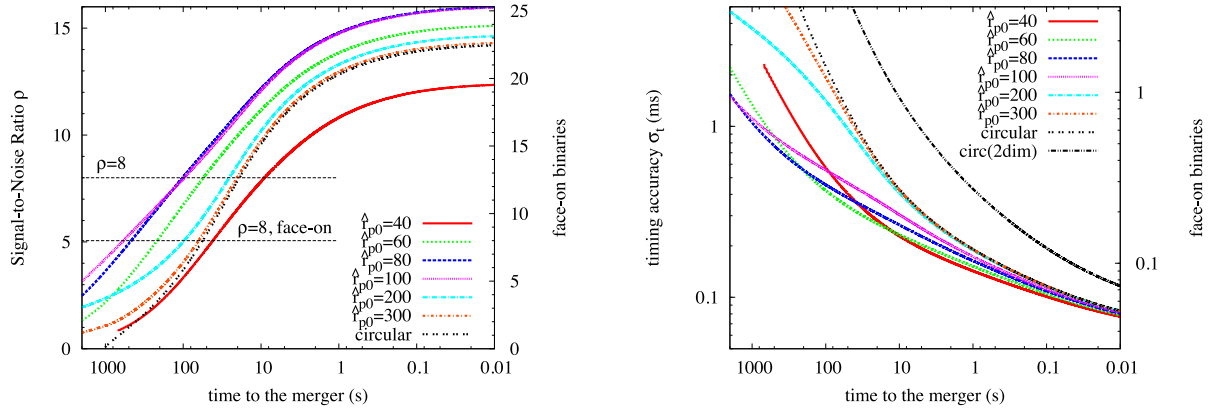

Figure 4. The time evolution of ρ and σ_t for a single detector with various values of $\hat{r}_{p0}$. The left and right axes correspond to the orientation-averaged and face-on binaries, respectively. All the values are for a 1.4–1.4 $M_\odot$ binary at $D = 100$ Mpc, and averaging over the sky position is always performed. Scalings are $\rho \propto D^{-1}$ and $\sigma_t \propto D$. Upper and lower horizontal lines in the left-hand panel show $\rho = 8$ for the orientation averaged and face-on cases, respectively. We include corresponding curves for the circular binaries, and also include timing accuracy obtained by the two-dimensional model as 'circ(2dim)'. In both plots, curves for $\hat{r}_{p0} = 40$ are artificially truncated at $e = e_{cut}(= 0.995)$, where $t_m(e_{cut}) \approx 800$ s.

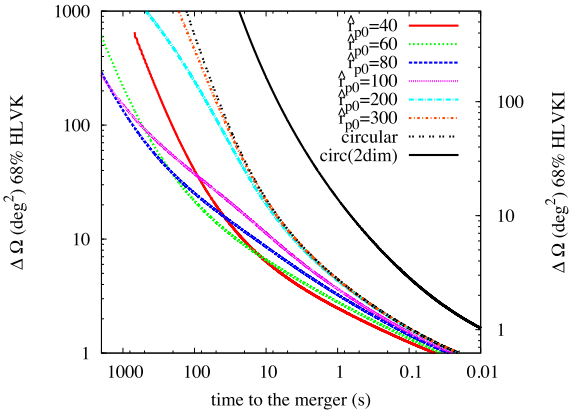

Figure 5. The time evolution of localization accuracy for various values of $\hat{r}_{p0}$, as well as that for a circular binary. The left and right axes are for LIGO Hanford-LIGO Livingston-Virgo-KAGRA network (HLVK) and the one with LIGO India (HLVKI), respectively. A 1.4–1.4 $M_\odot$ binary is assumed to be located at $D = 100$ Mpc, and a common value of σ_t (and implicitly ρ) is adopted for all the detectors for simplicity. We include a result obtained by the two-dimensional model of timing accuracy for a circular binary, and the realistic case may lie within the range between this curve and the one for the one-dimensional model (Grover et al. 2014).

Table 2. Localization accuracy $\Delta\Omega$ in deg^2 for various network configurations when σ_t is 1 ms at all the detectors. Recall that the localization accuracy scales as $\sigma_t^2[-\ln(1-p)]$ according to the confidence p. H, L, V, K, and I denote LIGO Hanford, LIGO Livingston, Virgo, KAGRA, and LIGO India, respectively. Detector locations are taken from Schutz (2011). The 'average' and 'worst' values for HLV are not shown, because the three detectors form a plane and localization accuracy is degraded by a factor of $1/\cos\Theta$ where Θ is the angle from the normal to this plane (Fairhurst 2011).

	HLV	HLVK	HLVI	HLVKI
68 per cent best	160	47	58	34
68 per cent average	–	120	120	76
68 per cent worst	–	330	360	190
90 per cent best	310	96	120	69
90 per cent average	–	250	240	150
90 per cent worst	–	660	720	380

confidence level are achieved. This should be contrasted with very large localization error for a circular binary, which will not enable us to declare that the source is localized in practice. The localization area is approximately halved if we restrict to 50 per cent confidence area, so that the five-detector network will be able to localize the source within $\sim$10 deg^2 even at 10 min before the merger.

Overheads of electromagnetic instruments would determine the required time to the merger if the latency associated with gravitational-wave data analysis could be reduced (Cannon et al. 2012). They depend on particular instruments, and one possibility may be 1 min which can be achieved with robotic telescopes such as Robotic Transient Search Experiment (Rykoff et al. 2005). The SNR exceeds 8 for various values of $\hat{r}_{p0}$, and the localization accuracy could be $\sim$10 deg^2 by the four-detector network with slightly lower confidence level than 68 per cent. This level of accuracy is expected only a few seconds before the merger for a circular binary. Although this assumption is too optimistic to be realistic, this reminds us that reducing the latency could have a practical impact on pre-merger localization accuracy of eccentric binaries.

The localization accuracy is better for a face-on binary, which may be a progenitor of an observable short-hard gamma-ray burst. The localization area for an eccentric binary is sufficient for typical gamma-ray satellites, such as *Fermi* Large Area Telescope (LAT), when $\rho = 8$ is achieved for a face-on one. This occurs earlier by an order of magnitude for an eccentric binary than for a circular binary (see Fig. 4). Still, taking not very rapid $\sim$0.2 deg s^{-1} slew speed of *Fermi*-LAT into account, a gamma-ray satellite capable of rapid timing-of-opportunity observation will be invaluable even if the sensitivity is inferior to current ones, because gamma-ray bursts at $O(100)$ Mpc should be extremely bright. The Large Size Telescopes of the Cherenkov Telescope Array will be able to perform rapid follow-up to observe more energetic photons at the GeV–TeV range, which may be able to distinguish mechanisms of the extended emission (Veres & Mészáros 2013).

5 SUMMARY AND DISCUSSION

We showed that gravitational waves from moderately eccentric compact binary coalescences will not only accumulate a substantial SNR at a few to 10 min before the merger, but also allow us to determine the sky position before the merger to the extent that we never

expect for circular compact binary coalescences. This unique property owes to higher mode gravitational waves emitted during the eccentric inspiral phase. The pre-merger localization could give us a way to observe the whole merger process and associated electromagnetic counterparts provided that the sum of the latency of sounding merger alerts and overheads of follow-up observation required by telescopes and satellites can be sufficiently reduced.

The gravitational radiation model adopted in this study is derived by the quadrupole formula with Newtonian two-point orbital dynamics (Peters & Mathews 1963; Peters 1964). Post-Newtonian corrections such as the periastron precession and spin-orbit interaction have to be taken into account for more quantitative study and actual data analysis (Brown & Zimmerman 2010; Huerta & Brown 2013), although theoretical templates of gravitational waves from eccentric compact binary coalescences are not developed very much compared to those for circular ones (e.g. Gopakumar & Schäfer 2011; Tessmer & Schäfer 2011). Tidal effects due to the finite size of neutron stars, such as the excitation of *f*-mode oscillation, will also become important at some stage of the orbital evolution (Stephens, East & Pretorius 2011; East & Pretorius 2012; Gold et al. 2012). We expect that these issues modify our conclusion only quantitatively, because the repeated pulse-like waveform at the early stage of inspiral is conserved. Another assuring point is that the waveform near the merger is irrelevant to the purpose of the pre-merger localization and merger alert, and thus higher order post-Newtonian and tidal effects should be safely neglected. As stated repeatedly, discontinuous orbital evolution in the high-eccentricity regime will require more careful consideration.

The timing triangulation approximation adopted in this study relies on the Fisher analysis, and it inevitably breaks down when we try to sound a merger alert using low SNR gravitational waves from a binary long before the merger. A detailed study such as Monte Carlo simulations is necessary to assess quantitatively the ability to localize the gravitational-wave source before the merger with low SNR signals. One important difference of the eccentric waveform from the circular one is the introduction of a new degree of freedom, which may be expressed as the angle of the periapsis direction (Barack & Cutler 2004). The correlation between this angle and timing accuracy has to be investigated quantitatively, whereas we expect that the timing accuracy primarily depends on the pulse-like waveform structure. In addition, a common value of the timing accuracy (and SNR) is adopted for all the detectors to derive the localization accuracy, and this approximation requires improvement.

A challenging task will be the matched filtering analysis for long-term gravitational-wave pulse sequences (see also Antonini, Murray & Mikkola 2014). In a pipeline of initial LIGO-Virgo data analysis, detector output data are usually split into 256 s segments (Babak et al. 2013). This will be lengthened in a pipeline of second-generation detectors, which are sensitive at lower frequency. The required segment length will be, however, much longer for eccentric binaries than for circular binaries if we try to process all the available information, because eccentric binaries emit detectable gravitational waves during their early lives with very low orbital frequency (see the end of Section 2). One way to overcome this is to develop a longer pipeline specialized to eccentric compact binary coalescences. The rotation of the earth will not be negligible with this strategy. Another way is to choose an appropriate time interval from the entire lifetime of an eccentric binary for a given length of the segment. The large number of harmonic modes can be a difficulty in practical construction of template banks without any dimensional reduction irrespective of the strategy.

The gravitational-wave pulse from an eccentric binary more resembles a detector glitch than the chirp signal from circular binaries does. Sequences of pulses may be naturally distinguished from noises by multidetector coincidences with information of timing consistency, and it might require human validation processes at least in the early epoch of second-generation gravitational-wave detectors. If high false alarm rates are allowed for the purpose of merger alerts to electromagnetic follow-up observations, omitting time consuming validation processes might be an option. Another, possibly ambitious, way to reduce effective latency might be to first carefully analyse gravitational-wave signals sufficiently before the merger aiming at rejecting false alarms, and next analyse signals as close to the merger as possible assuming that the signal is physical with available information from the first stage of analysis.

ACKNOWLEDGEMENTS

KK is deeply grateful to John L. Friedman for valuable discussions. KK is supported by JSPS Postdoctoral Fellowship for Research Abroad, and NS is supported by JSPS (24540269) and MEXT (24103006).

REFERENCES

Abadie J. et al., 2012, A&A, 539, A124
Accadia T. et al., 2011, Class. Quantum Gravity, 28, 025005
Antognini J. M., Shappee B. J., Thompson T. A., Amaro-Seoane P., 2014, MNRAS, 439, 1079
Antonini F., Perets H. B., 2012, ApJ, 757, 27
Antonini F., Murray N., Mikkola S., 2014, ApJ, 781, 45
Babak S. et al., 2013, Phys. Rev. D, 87, 024033
Barack L., Cutler C., 2004, Phys. Rev. D, 69, 082005
Berger E., 2013, preprint (arXiv:1311.2603)
Berger E., Fong W., Chornock R., 2013, ApJ, 774, L23
Bionta R. M., Blewitt G., Bratton C. B., Casper D., Ciocio A., 1987, Phys. Rev. Lett., 58, 1494
Brown D. A., Zimmerman P. J., 2010, Phys. Rev. D, 81, 024007
Cannon K. et al., 2012, ApJ, 748, 136
Cutler C., Flanagan É. É., 1994, Phys. Rev. D, 49, 2658
Cutler C., Kennefick D., Poisson E., 1994, Phys. Rev. D, 50, 3816
East W. E., Pretorius F., 2012, ApJ, 760, L4
East W. E., McWilliams S. T., Levin J., Pretorius F., 2013, Phys. Rev. D, 87, 043004
Evans P. A. et al., 2012, ApJS, 203, 28
Fairhurst S., 2009, New J. Phys., 11, 123006
Fairhurst S., 2011, Class. Quantum Gravity, 28, 105021
Flanagan É. É., Hughes S. A., 1998, Phys. Rev. D, 57, 4535
Gold R., Bernuzzi S., Thierfelder M., Brügmann B., Pretorius F., 2012, Phys. Rev. D, 86, 121501
Gopakumar A., Schäfer G., 2011, Phys. Rev. D, 84, 124007
Grover K., Fairhurst S., Farr B. F., Mandel I., Rodriguez C., Sidery T., Vecchio A., 2014, Phys. Rev. D, 89, 042004
Harry G. M. LIGO Scientific Collaboration, 2010, Class. Quantum Gravity, 27, 084006
Hirata K., Kajita T., Koshiba M., Nakahata M., Oyama Y., 1987, Phys. Rev. Lett., 58, 1490
Hotokezaka K., Kyutoku K., Tanaka M., Kiuchi K., Sekiguchi Y., Shiata M., Wanajo S., 2013, ApJ, 778, L16
Huerta E. A., Brown D. A., 2013, Phys. Rev. D, 87, 127501
Kasliwal M., Nissanke S., 2013, preprint (arXiv:1309.1554)
Kocsis B., Levin J., 2012, Phys. Rev. D, 85, 123005
Kyutoku K., Ioka K., Shibata M., 2014, MNRAS, 437, L6
Lee W. E., Ramirez-Ruiz E., van de Ven G., 2010, ApJ, 720, 953
LIGO Scientific Collaboration and Virgo Collaboration, 2013, preprint (arXiv:1304.0670)

Metzger B. D., Berger E., 2012, ApJ, 746, 48
Nakamura T., Kashiyama K., Nakauchi D., Suwa Y., Sakamoto T., Kawai N., 2013, preprint (arXiv:1312.0297)
Nakar E., 2007, Phys. Rep., 442, 166
Nissanke S., Kasliwal M., Georgieva A., 2013, ApJ, 767, 124
Nuttall L. K., Sutton P. J., 2010, Phys. Rev. D, 82, 102002
O'Leary R. M., Kocsis B., Loeb A., 2009, MNRAS, 395, 2127
Olver F. W. J., 1954, Phil. Trans. R. Soc. A, 247, 328
Peters P. C., 1964, Phys. Rev., 136, B1224
Peters P. C., Mathews J., 1963, Phys. Rev., 131, 435
Piran T., Nakar E., Rosswog S., 2013, MNRAS, 430, 2121
Rykoff E. S. et al., 2005, ApJ, 631, L121
Samsing J., Macleod M., Ramirez-Ruiz E., 2014, ApJ, 784, 71
Schutz B. F., 1986, Nature, 323, 310
Schutz B. F., 2011, Class. Quantum Gravity, 28, 125023
Seto N., 2013, Phys. Rev. Lett., 111, 061106
Somiya K., 2012, Class. Quantum Gravity, 29, 124007
Stephens B. C., East W. E., Pretorius F., 2011, ApJ, 737, L5
Tanvir N. R., Levan A. J., Fruchter A. S., Hjorth J., Hounsell R., Wiersema K., Tunnicliffe R. L., 2013, Nature, 500, 547
Tessmer M., Schäfer G., 2011, Ann. Phys., 523, 813
Tsang D., 2013, ApJ, 777, 103
Veres P., Mészáros P., 2013, preprint (arXiv:1312.0590)

APPENDIX A: FISHER ANALYSIS

We compute the Fisher information matrix $\Gamma_{\alpha\beta}$ with respect to t_0 and Φ_0, where Greek indices take t for t_0 or Φ for Φ_0. Using the fact that the nth harmonic mode is proportional to $\exp[in(2\pi f_{\rm orb}t_0 - \Phi_0)]$ in the frequency domain, we can replace differentiation with respect to t_0 and Φ_0 by multiplication of $2\pi i f_n$ and $-in$, respectively (Cutler & Flanagan 1994). Components of the Fisher matrix are given by

$$\Gamma_{tt} = (2\pi)^2 \sum_{n=1}^{\infty} \rho_n^2 \overline{f_n^2}, \tag{A1}$$

$$\Gamma_{t\Phi} = \Gamma_{\Phi t} = -2\pi \sum_{n=1}^{\infty} n\rho_n^2 \overline{f_n}, \tag{A2}$$

$$\Gamma_{\Phi\Phi} = \sum_{n=1}^{\infty} n^2 \rho_n^2. \tag{A3}$$

Computing the inverse of this two-dimensional Fisher information matrix, we obtain the expression of the timing accuracy,

$$\sigma_{\rm t} = \frac{1}{2\pi} \sqrt{\frac{\sum_n n^2\rho_n^2}{(\sum_m \rho_m^2 \overline{f_m^2})(\sum_n n^2\rho_n^2) - (\sum_n n\rho_n^2 \overline{f_m})^2}}. \tag{A4}$$

Note that for a circular binary emitting only via the $n = 2$ mode, this expression gives

$$\sigma_{{\rm t},s} = \frac{1}{2\pi\rho\sigma_{f,s}}, \tag{A5}$$

where $\sigma_{f,s}^2 \equiv \overline{f_2^2} - \overline{f_2}^2$ is the effective bandwidth for single, $n = 2$ mode gravitational waves. This result agrees with the one derived in Fairhurst (2009).

Now, let us confirm the divergence of phase-related components using a simplified detector model characterized by

$$\frac{1}{S(f)} = \frac{\delta(f - f_{\rm obs})}{S}, \tag{A6}$$

where S is a constant. The SNR is given by

$$\rho^2 \propto \sum_n \int \frac{|{\rm d}E_n/{\rm d}f_n|}{f_n^2 S(f_n)} {\rm d}f_n, \tag{A7}$$

and thus, we have

$$\rho^2 \propto \sum_n \frac{1}{f_{\rm obs}^2 S} \left|\frac{{\rm d}E_n}{{\rm d}f_n}\right|_{f_n = f_{\rm obs}}. \tag{A8}$$

Hereafter, we replace $\sum_n$ by an integral and express the luminosity in a more convenient form as

$$\rho^2 \propto \int \left[\frac{1}{f_{\rm obs}^2 S} \frac{{\rm d}E_n}{{\rm d}t} \left(\frac{{\rm d}e}{{\rm d}t}\right)^{-1} \left(\frac{{\rm d}f_n}{{\rm d}e}\right)^{-1}\right]_{f_n = f_{\rm obs}} {\rm d}n. \tag{A9}$$

In the limit of $e \to 1$, we have

$$a \propto (1-e)^{-1}, \tag{A10}$$

$$f_{\rm orb} \propto a^{-3/2} \propto (1-e)^{3/2}, \tag{A11}$$

$$\frac{{\rm d}E_n}{{\rm d}t} \propto \frac{g(n,e)}{a^5} \propto g(n,e)(1-e)^5, \tag{A12}$$

$$\frac{{\rm d}e}{{\rm d}t} \propto \frac{1}{a^4(1-e)^{5/2}} \propto (1-e)^{3/2}, \tag{A13}$$

$$\frac{{\rm d}f_n}{{\rm d}e} = n\frac{{\rm d}f_{\rm orb}}{{\rm d}e} \propto n(1-e)^{1/2}. \tag{A14}$$

Therefore, the SNR is approximately written as

$$\rho^2 \propto \int \left[\frac{g(n,e)}{n}(1-e)^3\right] {\rm d}n. \tag{A15}$$

Now we can relate n and $1 - e$ by $f_{\rm obs} = nf_{\rm orb}(e)$ as

$$n \propto (1-e)^{-3/2}\ ,\ (1-e) \propto n^{-2/3}, \tag{A16}$$

and we can derive (Olver 1954)

$$g(n, e(n)) \propto n^{4/3} \tag{A17}$$

at the limit of $n \to \infty$ ($e \to 1$). Finally, we have

$$\rho^2 \propto \int n^{-5/3} {\rm d}n. \tag{A18}$$

Thus, the integral (or originally the summation) of ρ^2 is not divergent at $e \to 1$, so is Γ_{tt}. The integral for $\Gamma_{t\Phi} \propto \sum n\rho_n^2$ diverges but as moderate as $n(e)^{1/3}$. The integral for $\Gamma_{\Phi\Phi} \propto \sum n^2\rho_n^2$ is $n(e)^{4/3}$, and thus violent.

This paper has been typeset from a TEX/LATEX file prepared by the author.